

In situ calibrated angle between the quantization axis and the propagating direction of the light field for trapping neutral atoms

Rui-Jun Guo(郭瑞军), Xiao-Dong He(何晓东), Cheng Sheng(盛诚), Kun-Peng Wang(王坤鹏), Peng Xu(许鹏), Min Liu(刘敏), Jin Wang(王谨), Xiao-Hong Sun(孙晓红), Yong Zeng(曾勇), and Ming-Sheng Zhan(詹明生)
Citation: Chin. Phys. B, 2024, 33 (**2**): 023701. DOI: 10.1088/1674-1056/acf11d
Journal homepage: http://cpb.iphy.ac.cn; http://iopscience.iop.org/cpb

What follows is a list of articles you may be interested in

Quantum degenerate Bose-Fermi atomic gas mixture of ^{23}Na and ^{40}K

Ziliang Li(李子亮), Zhengyu Gu(顾正宇), Zhenlian Shi(师振莲), Pengjun Wang(王鹏军), and Jing Zhang(张靖)
Chin. Phys. B, 2023, 32 (**2**): 023701. DOI: 10.1088/1674-1056/aca14f

Superfluid to Mott-insulator transition in a one-dimensional optical lattice

Wenliang Liu(刘文良), Ningxuan Zheng(郑宁宣), Jun Jian(蹇君), Li Tian(田丽), Jizhou Wu(武寄洲), Yuqing Li(李玉清), Yongming Fu(付永明), Peng Li(李鹏), Vladimir Sovkov, Jie Ma(马杰), Liantuan Xiao(肖连团), and Suotang Jia(贾锁堂)
Chin. Phys. B, 2022, 31 (**7**): 073702. DOI: 10.1088/1674-1056/ac6579

Cold atom clocks and their applications in precision measurements

Shao-Yang Dai(戴少阳), Fa-Song Zheng(郑发松), Kun Liu(刘昆), Wei-Liang Chen(陈伟亮), Yi-Ge Lin(林弋戈), Tian-Chu Li(李天初), and Fang Fang(房芳)
Chin. Phys. B, 2021, 30 (**1**): 013701. DOI: 10.1088/1674-1056/abbbee

Dynamical properties of ultracold Bose atomic gases in one-dimensional optical lattices created by two schemes

Jiang Zhu(朱江), Cheng-Ling Bian(边成玲), Hong-Chen Wang(王红晨)
Chin. Phys. B, 2019, 28 (**9**): 093701. DOI: 10.1088/1674-1056/ab3448

Comparison of single-neutral-atom qubit between in bright trap and in dark trap

Ya-Li Tian(田亚莉), Zhi-Hui Wang(王志辉), Peng-Fei Yang(杨鹏飞), Peng-Fei Zhang(张鹏飞), Gang Li(李刚), Tian-Cai Zhang(张天才)
Chin. Phys. B, 2019, 28 (**2**): 023701. DOI: 10.1088/1674-1056/28/2/023701

In situ calibrated angle between the quantization axis and the propagating direction of the light field for trapping neutral atoms

Rui-Jun Guo(郭瑞军)[1], Xiao-Dong He(何晓东)[2], Cheng Sheng(盛诚)[2], Kun-Peng Wang(王坤鹏)[2], Peng Xu(许鹏)[2], Min Liu(刘敏)[2], Jin Wang(王谨)[2], Xiao-Hong Sun(孙晓红)[1], Yong Zeng(曾勇)[1,†], and Ming-Sheng Zhan(詹明生)[2]

[1] *Henan Key Laboratory of Laser and Optoelectronic Information, National Center for International Joint Research of Electronic Materials and Systems, School of Electrical and Information Engineering, Zhengzhou University, Zhengzhou* 450001, *China*

[2] *State Key Laboratory of Magnetic Resonance and Atomic and Molecular Physics, Innovation Academy for Precision Measurement Science and Technology, Chinese Academy of Sciences, Wuhan* 430071, *China*

(Received 29 April 2023; revised manuscript received 23 July 2023; accepted manuscript online 17 August 2023)

The recently developed magic-intensity trapping technique of neutral atoms efficiently mitigates the detrimental effect of light shifts on atomic qubits and substantially enhances the coherence time. This technique relies on applying a bias magnetic field precisely parallel to the wave vector of a circularly polarized trapping laser field. However, due to the presence of the vector light shift experienced by the trapped atoms, it is challenging to precisely define a parallel magnetic field, especially at a low bias magnetic field strength, for the magic-intensity trapping of ^{85}Rb qubits. In this work, we present a method to calibrate the angle between the bias magnetic field and the trapping laser field with the compensating magnetic fields in the other two directions orthogonal to the bias magnetic field direction. Experimentally, with a constant-depth trap and a fixed bias magnetic field, we measure the respective resonant frequencies of the atomic qubits in a linearly polarized trap and a circularly polarized one via the conventional microwave Rabi spectra with different compensating magnetic fields and obtain the corresponding total magnetic fields via the respective resonant frequencies using the Breit–Rabi formula. With known total magnetic fields, the angle is a function of the other two compensating magnetic fields. Finally, the projection value of the angle on either of the directions orthogonal to the bias magnetic field direction can be reduced to $0(4)^\circ$ by applying specific compensating magnetic fields. The measurement error is mainly attributed to the fluctuation of atomic temperature. Moreover, it also demonstrates that, even for a small angle, the effect is strong enough to cause large decoherence of Rabi oscillation in a magic-intensity trap. Although the compensation method demonstrated here is explored for the magic-intensity trapping technique, it can be applied to a variety of similar precision measurements with trapped neutral atoms.

Keywords: quantization axis, trapping laser, angle, compensating magnetic fields

PACS: 37.10.Jk **DOI:** 10.1088/1674-1056/acf11d

1. Introduction

Single neutral atoms in tightly focused optical dipole traps (ODTs) are being intensively developed for studies of quantum simulation[1,2] and quantum computation.[3–6] A practical quantum simulator or computer relies on coherent manipulation of quantum bits (qubits). Moreover, coherence times are of great importance for applications in the fields of quantum metrology[7–9] and precision measurements.[10] Although atomic states have excellent coherence properties in an isolated environment, the inherent differential light shifts (DLSs) of neutral atoms in optical tweezers induced by the trapping laser field cause a strong inhomogeneous dephasing effect.[11–14] To suppress this detrimental effect, a magic-intensity trapping technique was developed recently[15] and used extensively.[16–18]

In order to create effective magic-intensity trapping for microwave clock transitions, an external bias magnetic field $\boldsymbol{B}_{\rm bias}$ is arranged to be strictly parallel to the circularly polarized trapping laser field. In this way, the trapping laser field induces a fourth-order hyperpolarizability β_4 that is expressed in terms of the degree of circular polarization, hyperfine splitting and the vector polarizability of the ground state, which makes the DLS dependence on the trapping laser intensity parabolic. Owing to the parabolic dependence, at a magic-intensity trap depth, the first-order sensitivity of the DLS to the trapping laser intensity variations from the whole ODT volume is eliminated so that the coherence time of ^{87}Rb qubits is substantially enhanced[15] and the coherence times of the mixed-isotope qubits are substantially enhanced and balanced to be nearly 1 s.[18] Different from the widely used linear polarization trapping laser, for atoms in the circularly or elliptically polarized magic-intensity ODTs, trapping laser fields in general give rise to vector light shifts that are equivalent to the effect of a fictitious magnetic field $\boldsymbol{B}_{\rm fict}$[19–30] scaling linearly with the trap depth. If the $\boldsymbol{B}_{\rm bias}$ defined quantization axis is not aligned with the trapping laser, the total magnetic field combined with $\boldsymbol{B}_{\rm fict}$ and $\boldsymbol{B}_{\rm bias}$ will vary with the trap depth. During the measurement of the DLS parabolic curve by conven-

†Corresponding author. E-mail: ieyzeng@zzu.edu.cn

© 2024 Chinese Physical Society and IOP Publishing Ltd

tional Ramsey interferometry for the magic-intensity trapping of ^{85}Rb qubits, microwave radiation is used to coherently manipulate the clock transitions of the ground states. With a fixed microwave antenna, the projection value of microwave power on the total magnetic field also varies with the trap depths, resulting in an inconsistency of Rabi frequencies between the ground states in ODTs with different trap depths. In turn, the difference in Rabi frequencies leads to imperfect measurements of the conventional Ramsey interferometry, which is detrimental to the accurate measurement of hyperpolarizability. In addition, fluctuations of the microwave power may also cause large errors in the coherent manipulation of single qubits in the magic-intensity ODT array.[16] Therefore, it is crucial to calibrate the angle accurately.

Since it is difficult to accurately measure the magnetic fields in the ODTs by using a traditional magnetometer, researchers have developed *in situ* measurement methods to measure the magnetic field vector. In the study of optically parallel readout of multiple qubits with high fidelity, the presence of atoms and their internal states are minimally altered by utilizing a circular polarization probe laser.[31,32] It is required that the propagation direction of the probe laser must be strictly aligned with the quantization axis. A procedure adapted from Ref. [33] was used to minimize the angle, which uses the atoms themselves as probes to optimize the magnetic field vector. The quantization axis is created by $\boldsymbol{B}_{\rm bias}$ along the Z direction, further adjustment of the magnetic field by the X–Y compensating magnetic fields is required. The ^{87}Rb qubits are first optically pumped to $|F=2, m_F=2\rangle$ by a circularly polarized beam. One of the σ_+-polarized probe lasers is tuned to $|2\rangle \leftrightarrow |2'\rangle$ and optically pumps the qubits into the dark state $|2, 2\rangle$. When the alignment is optimal, the dark state $|2, 2\rangle$ can only couple off-resonantly to $|3', 3'\rangle$. If there is any mismatch, the dark state $|2, 2\rangle$ mixes with the bright states and scatters photons, eventually depumping into $|1\rangle$, which can be measured by the destructive blow-away measurement. The optimum values for the X–Y compensating magnetic fields were experimentally optimized by minimizing the survival probability such that only 13% of the qubits are transferred to $|1\rangle$. In this *in situ* method they did not quantify the relationship between the angle and the X–Y compensating magnetic fields for further adjustment of the quantization axis. Herein, we present an *in situ* method to quantitatively calibrate the angle between the quantization axis and the trapping laser with the compensating magnetic fields in the other two directions orthogonal to the $\boldsymbol{B}_{\rm bias}$ direction.

This paper is organized as follows. We first briefly describe the compensation method. Subsequently, we introduce the experimental setup for building an ODT to confine a single ^{85}Rb qubit and show the spatial position of the magnetic fields. Then, we make use of the qubits as sensitive probes to measure the respective resonant frequencies of the atomic qubits in linearly and circularly polarized ODTs via conventional microwave Rabi spectra with different compensating magnetic fields and obtain the corresponding total magnetic fields via the respective resonant frequencies using the Breit–Rabi formula. With known total magnetic fields, the relationship between the angle and the other two compensating magnetic fields is quantitatively obtained. Finally, we perform a comparative experiment to verify the differences between the calibrated and uncalibrated angles and the calibration accuracy of the *in situ* compensating technique.

2. Experimental methods

As the idea of a fictitious magnetic field will be of great importance to understand the compensating technique, we will discuss this concept in detail. The ODTs rely on the intensity-dependent energy shift of the atomic ground state for an atom exposed to a trapping laser field, which is far-detuned with respect to the atomic transitions of D lines. For an alkali-metal atom in the ground state, the interaction Hamiltonian can be approximated as[19,25,27]

$$\widehat{\boldsymbol{V}} = -\frac{1}{4}\alpha_{\rm s}|\boldsymbol{\varepsilon}|^2 + {\rm i}\alpha_{\rm v}\frac{[\boldsymbol{\varepsilon}^*\times\boldsymbol{\varepsilon}]\cdot\widehat{\boldsymbol{F}}}{8F}, \tag{1}$$

where $\alpha_{\rm s}$ and $\alpha_{\rm v}$ are the scalar and vector polarizabilities, respectively, $\boldsymbol{\varepsilon} = \varepsilon\boldsymbol{u}$ with ε and $\boldsymbol{u}$ being the field amplitude and the polarization vector, respectively, and F is the quantum number for the total angular momentum. The effect of the vector light shift is equivalent to having an extra magnetic field, which is called a fictitious magnetic field $\boldsymbol{B}_{\rm fict}$. We obtain an induction field by equating the shift to Zeeman shift

$${\rm i}\alpha_{\rm v}\frac{[\boldsymbol{\varepsilon}^*\times\boldsymbol{\varepsilon}]\cdot\widehat{\boldsymbol{F}}}{8F} = g_{\rm F}\mu_{\rm B}\boldsymbol{B}_{\rm fict}\cdot\widehat{\boldsymbol{F}}. \tag{2}$$

Thus the equivalent $\boldsymbol{B}_{\rm fict}$ is given by

$$\boldsymbol{B}_{\rm fict} = {\rm i}\alpha_{\rm v}\frac{[\boldsymbol{\varepsilon}^*\times\boldsymbol{\varepsilon}]}{8g_{\rm F}\mu_{\rm B}F}, \tag{3}$$

with $\mu_{\rm B}$ as the Bohr magneton and $g_{\rm F}$ as the hyperfine Lande factor. The direction of the $\boldsymbol{B}_{\rm fict}$ is determined by the light field vector ${\rm i}[\boldsymbol{\varepsilon}^*\times\boldsymbol{\varepsilon}]$, which is a real vector. Similar to a real magnetic field, the $\boldsymbol{B}_{\rm fict}$ flips under time reversal. The maximal magnitude of the term ${\rm i}[\boldsymbol{\varepsilon}^*\times\boldsymbol{\varepsilon}]$ is obtained with a fully circularly polarized ODT and is zero for a linearly polarized trapping field. It is convenient to express the shift in terms of the mean trap depth for ground states as $U_{\rm a} = -1/4\alpha_{\rm s}|\boldsymbol{\varepsilon}|^2$. For the ground state of ^{85}Rb qubits in an 830 nm circularly polarized ODT, we calculate $\boldsymbol{B}_{\rm fict} = -0.10(1)$ (G/MHz)$\cdot U_{\rm a}$.

For an atom in the electronic ground state, the fictitious magnetic field behaves in almost every respect like a real magnetic field. When an atom is in the hybrid real–fictitious field, the total amplitude and direction of the field are under the rule of vector operation. Thus, the $\boldsymbol{B}_{\rm fict}$ can be vector-added to the

real magnetic field $\boldsymbol{B}_{\rm real}$, such that the atom is in total exposed to the effective magnetic field $\boldsymbol{B}_{\rm eff} = \boldsymbol{B}_{\rm fict} + \boldsymbol{B}_{\rm real}$, which has been found in early works.[19,25,26,28,29] This was further supported in various experiments, demonstrating, for example, optically induced spin precession and echoes in an atomic beam,[20,21] an optical Stern–Gerlach effect from Zeeman-like ac Stark shift,[22,30] and an optically induced fictitious magnetic trap on an atom chip.[23]

In our experiment, we define the propagation direction of the circularly polarized trapping laser to be Z-axis, which is also the direction of $\boldsymbol{B}_{\rm fict}$. The axis of the Helmholtz coil producing $\boldsymbol{B}_{\rm bias}$ is not perfectly aligned with the propagation direction of the trapping laser, as shown in Fig. 1, so that the quantization axis created by the $\boldsymbol{B}_{\rm bias}$ is not parallel to the trapping laser. Further adjustment of the quantization axis by the compensating magnetic fields $\boldsymbol{B}_x$ and $\boldsymbol{B}_y$ in the other two directions orthogonal to the $\boldsymbol{B}_{\rm bias}$ direction created by compensating Helmholtz coils are required. Here, the three-axle magnetic fields created by the Helmholtz coils are collectively referred to as the external magnetic field $\boldsymbol{B}_{\rm ext}$. The total magnetic field $\boldsymbol{B}_{\rm tot}$ in a circularly polarized trapping light field is given by the expression

$$\boldsymbol{B}_{\rm tot} = \boldsymbol{B}_{\rm ext} + \boldsymbol{B}_{\rm fict}. \tag{4}$$

The square of the magnitude of the magnetic vector $\boldsymbol{B}_{\rm tot}$ is written as

$$\begin{aligned} |\boldsymbol{B}_{\rm tot}|^2 &= |\boldsymbol{B}_{\rm ext} + \boldsymbol{B}_{\rm fict}|^2 \\ &= |\boldsymbol{B}_{\rm ext}|^2 + |\boldsymbol{B}_{\rm fict}|^2 + 2|\boldsymbol{B}_{\rm ext}||\boldsymbol{B}_{\rm fict}|\cos(\theta), \end{aligned} \tag{5}$$

thus $\cos(\theta)$ is given by

$$\cos(\theta) = \frac{|\boldsymbol{B}_{\rm tot}|^2 - |\boldsymbol{B}_{\rm ext}|^2 - |\boldsymbol{B}_{\rm fict}|^2}{2|\boldsymbol{B}_{\rm ext}||\boldsymbol{B}_{\rm fict}|}, \tag{6}$$

where θ is the angle between the $\boldsymbol{B}_{\rm ext}$ and $\boldsymbol{B}_{\rm fict}$, as shown in Fig. 1. This θ is exactly the angle between the quantization axis and the direction of the trapping laser. When $\varphi = 0^\circ$, the projection value of θ on the Z–X plane is expressed as θ_x, which can be calibrated by the $\boldsymbol{B}_x$. Similarly, when $\varphi = 90^\circ$, the projection value of θ on the Z–Y plane is expressed as θ_y, which can be calibrated by the $\boldsymbol{B}_y$. Equation (6) can be resolved into the following two parts with the parameters

$$\theta_x = \arccos\left[\frac{|\boldsymbol{B}_{\rm tot}(B_{\rm bias}, B_x, B_{\rm fict})|^2 - |\boldsymbol{B}_{\rm ext}(B_{\rm bias}, B_x)|^2 - |\boldsymbol{B}_{\rm fict}|^2}{2|\boldsymbol{B}_{\rm ext}(B_{\rm bias}, B_x)||\boldsymbol{B}_{\rm fict}|}\right], \tag{7}$$

$$\theta_y = \arccos\left[\frac{|\boldsymbol{B}_{\rm tot}(B_{\rm bias}, B_y, B_{\rm fict})|^2 - |\boldsymbol{B}_{\rm ext}(B_{\rm bias}, B_y)|^2 - |\boldsymbol{B}_{\rm fict}|^2}{2|\boldsymbol{B}_{\rm ext}(B_{\rm bias}, B_y)||\boldsymbol{B}_{\rm fict}|}\right]. \tag{8}$$

For a given trap depth, the $\boldsymbol{B}_{\rm fict}$ is a constant. Therefore, the angle is stated as a function of the $\boldsymbol{B}_{\rm ext}$ and $\boldsymbol{B}_{\rm tot}$. Experimentally, the qubits serve as sensitive probes for measuring the $\boldsymbol{B}_{\rm ext}$ and $\boldsymbol{B}_{\rm tot}$, which are inherently dependent on the resonance frequencies of Zeeman-sensitive spectral transition. The $\boldsymbol{B}_{\rm ext}$ ($\boldsymbol{B}_{\rm tot}$) can be accurately extracted from the measured resonance frequency of Zeeman-sensitive spectral transition in the linearly (fully circularly) polarized trap. Different values of θ_x (θ_y) are obtained by varying the $\boldsymbol{B}_x$ ($\boldsymbol{B}_y$). The relationship between θ_x (θ_y) and $\boldsymbol{B}_x$ ($\boldsymbol{B}_y$) is quantitatively obtained.

3. Experimental setup

Figure 1 depicts the experimental setup and the spatial position of the magnetic fields. The trapping laser propagates along $\boldsymbol{k}_{\rm ODT}$, the long axis of the ODT, which is set to be the Z-axis. In a circularly polarized ODT, the $\boldsymbol{k}_{\rm ODT}$ is also the direction of the $\boldsymbol{B}_{\rm fict}$. The $\boldsymbol{B}_{\rm ext}$, making a polar angle θ from the Z-axis and an azimuthal angle φ from the X-axis, is combined with $\boldsymbol{B}_x$, $\boldsymbol{B}_y$ and $\boldsymbol{B}_{\rm bias}$ for shifting the atomic ensemble and defining the quantization axis. The projection value of θ onto the Z–X (Z–Y) plane is expressed as θ_x (θ_y) by setting $\varphi = 0^\circ$ (90°). The θ_x (θ_y) can be calibrated by applying the $\boldsymbol{B}_x$ ($\boldsymbol{B}_y$), which is linear with the compensating Helmholtz coil current $X_{\rm current}$ ($Y_{\rm current}$). The ^{85}Rb qubits are rotated by microwave radiation, which is sent through a microwave antenna that is placed at a fixed distance of 4 cm away from the ODT. The experimental details on trapping and manipulating a single ^{85}Rb qubit have been described in our previous work.[18] In brief, the single atom for encoding quantum logical state is obtained by loading it into an 830 nm ODT directly from a magneto-optical trap (MOT) based on collisional blockade mechanism.[34,35] When a single atom is detected, it is further cooled to about 14 μK with the standard optical molasses method in linearly polarized ODT with trap depth of 0.4 mK. We note that the polarization of the trapping laser is actively engineered by incorporating a liquid crystal retarder. Then the trapped atom is initialized into the hyperfine state of $|0\rangle \equiv |5s_{1/2}, F = 2, m_F = 0\rangle$ with optical pumping. For the state-selective detection after the manipulating, a circularly polarized probe laser beam resonant with the transition between $|5s_{1/2}, F = 3\rangle$ and $|5p_{3/2}, F = 4\rangle$ is applied to push out the atoms in the state $|5s_{1/2}, F = 3\rangle$. Whereas, the atoms in the state $|5s_{1/2}, F = 2\rangle$ remain in the trap and contribute to the fluorescence, which is collected by a single-photon counting module.

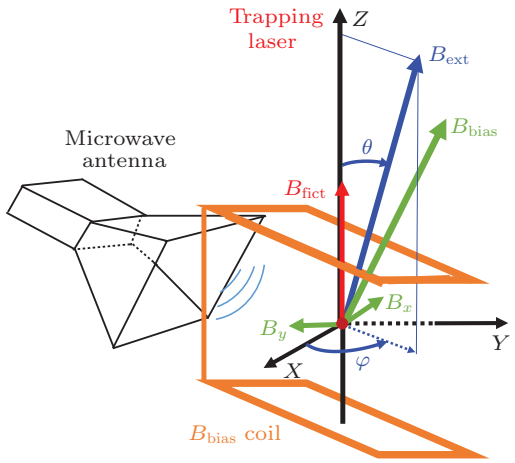


Fig. 1. Experimental setup and spatial position of the magnetic fields. The ^{85}Rb atom (red dot) is trapped in an 830 nm ODT and coherently manipulated with microwave radiation from a horn outside the vacuum cell. The bias magnetic field $\boldsymbol{B}_{\rm bias}$ is created by a leaning Helmholtz coil. The compensating magnetic fields $\boldsymbol{B}_x$ and $\boldsymbol{B}_y$ are also created by Helmholtz coils, which are not shown here. The direction of the external magnetic field $\boldsymbol{B}_{\rm ext}$ (blue line) can point in any direction by changing the $\boldsymbol{B}_x$ and $\boldsymbol{B}_y$. Note that the magnetic field values and the angle shown here are not strictly to scale.

4. Results and discussion

For our compensation experiment, each experimental sequence starts by loading atoms into the MOT and transferring them to the ODTs. Assuming that the trap depth is shallow, the effect of $\boldsymbol{B}_{\rm fict}$ is not obvious. On the contrary, if the trap depth is deeper, the atoms in the ODTs experience a higher temperature, leading to an inhomogeneous light shift broadening of the microwave spectrum for a ground-state hyperfine transition. Therefore, the typical parameter for our trap depth is $h\times(-1.2\ \text{MHz})$.

Taking the $\boldsymbol{B}_{\rm bias}$ to be about 0.60 G with a fixed Helmholtz coil current, we measure the dependence of θ_x on the compensating Helmholtz coil current $X_{\rm current}$. Firstly, we set 40 mA for $Y_{\rm current}$, which is an estimated value for $\varphi=0°$, and measure the microwave resonant frequencies between Zeeman-sensitive hyperfine states $|0\rangle$ and $|5s_{1/2}, F=3, m_F=1\rangle$ in linearly and circularly polarized ODTs. The microwave spectroscopy is driven by microwave radiation at varying frequencies around 3.036 GHz. With eight different values of $X_{\rm current}$, eight sets of microwave resonant frequencies are measured, as shown in Fig. 2(a). Then, eight corresponding groups of $\boldsymbol{B}_{\rm ext}$ ($\boldsymbol{B}_{\rm tot}$) in linearly (fully circularly) polarized ODTs, as shown in Fig. 2(b), are extracted from the microwave resonant frequencies by using the Breit–Rabi formula ($\Delta E_{\rm mag}(x)=\Delta E_{\rm HFS}[a_1 M_F x\pm\frac{1}{2}\sqrt{1+\frac{4M_F}{2I+1}c_1 x+c_2 x^2}$ $(x=\mu_0 B/\Delta E_{\rm HFS}))$[36,37] for sublevels of the two hyperfine ground states. When the difference between $B_{\rm ext}$ and $B_{\rm tot}$ reaches the maximum, the $\boldsymbol{B}_{\rm ext}$ is parallel to the trapping laser. We obtain that the $\boldsymbol{B}_{\rm fict}=\boldsymbol{B}_{\rm tot}-\boldsymbol{B}_{\rm ext}$ is 0.12(2) G, which is consistent with the theoretical result $\boldsymbol{B}_{\rm fict}=-0.10(1)\ (\text{G/MHz})\times U_{\rm a}=0.12(1)$ G. Finally, substituting the fitted values of $\boldsymbol{B}_{\rm ext}$ and $\boldsymbol{B}_{\rm tot}$ under the same $X_{\rm current}$ into Eq. (7) yields the dependence of θ_x on $X_{\rm current}$, which is shown in Fig. 2(c) with purple squares. The θ_x scales linearly with the $X_{\rm current}$, and the fitted equation is $\theta_x=-0.20(1)\ (°/\text{mA})\times X_{\rm current}+23(4)°$. According to this equation, we obtain that the calibrated value of θ_x is 23(4)°. When $X_{\rm current}$ is 115 mA, θ_x is compensated to 0(4)°, which means that the quantization axis is parallel to the trapping laser.

Accordingly, setting 115 mA for $X_{\rm current}$, seven sets of microwave resonant frequencies are measured, as shown in Fig. 2(d). The fitted values of $\boldsymbol{B}_{\rm ext}$ and $\boldsymbol{B}_{\rm tot}$ under the same $Y_{\rm current}$, as shown in Fig. 2(e), are collected in the same way as above. The maximum difference between $B_{\rm ext}$ and $B_{\rm tot}$ is 0.12(0) G, which is also consistent with the theoretical result 0.12(1) G. Then, the dependence of θ_y on $Y_{\rm current}$, which is shown in Fig. 2(f) with pink circles, is obtained though Eq. (8). The θ_y scales linearly with $Y_{\rm current}$, and the fitted equation is $\theta_y=-0.28(1)(°/\text{mA})\times Y_{\rm current}+9(2)°$. From this equation, we obtain that the original θ_y is 9(2)°. When $Y_{\rm current}$ is 32 mA, θ_y is compensated to 0(4)°.

In our experimental system, the calculated values of θ_x and θ_y are 23(4)° and 9(2)°, respectively. With known θ_x (θ_y), we can obtain the projection value of any $\boldsymbol{B}_{\rm bias}$ in the other two directions orthogonal to the $\boldsymbol{B}_{\rm bias}$ direction and eliminate the θ_x (θ_y) by applying the compensating magnetic field $\boldsymbol{B}_x$ ($\boldsymbol{B}_y$) in the equivalent direction. Naturally, the compensating current $X_{\rm current}$ ($Y_{\rm current}$) is obtained based on the linear relationship between the compensating magnetic field $\boldsymbol{B}_x$ ($\boldsymbol{B}_y$) and the compensating Helmholtz coil current $X_{\rm current}$ ($Y_{\rm current}$). In addition, an estimation of the angle between the other two compensating magnetic fields $\boldsymbol{B}_x$ and $\boldsymbol{B}_y$ is (90±10)°, which is obtained by comparing the $\boldsymbol{B}_{\rm fict}$ from Figs. 2(b) and 2(e).

To understand the sources contributing to the above-accumulated error of θ_x (θ_y), we examine four main sources of error during the measurement of the magnetic fields in our experiment.

(1) **The temperature fluctuation of the atoms** As a thermal ensemble with the temperature of $T_{\rm a}$, the atoms possess an average potential energy of $3\kappa_{\rm B}T_{\rm a}/2$. The average trap depth $U_{\rm a}$ seen by the thermal atoms fulfills $U_{\rm a}=hU_0+3\kappa_{\rm B}T_{\rm a}/2$, where U_0 is the dipole potential at the bottom of the trap. During the experimental sequence, the temperature with a fluctuation of 10% is obtained using the release and recapture method. It introduces a 3% fluctuation in the $\boldsymbol{B}_{\rm fict}$, which is proportional to the trap depth $U_{\rm a}$. So the maximum fluctuation of the $\cos(\theta)$ is 3%, which is the same order of magnitude as the calculated value of θ_x (θ_y).

(2) **Fluctuations in the background magnetic field** Using a flux-gate magnetometer, we measured a peak-to-peak value of the magnetic field (with fluctuations of $\sim$ 1.0 mG)

dominated by components at 50 Hz. This fluctuation of the background magnetic field in all directions introduces 1% fluctuation of $\boldsymbol{B}_{\rm fict}$ and 1‰ fluctuation of $\boldsymbol{B}_{\rm ext}$. These parameters introduce the maximal fluctuation of the $\cos(\theta)$ up to 15‰.

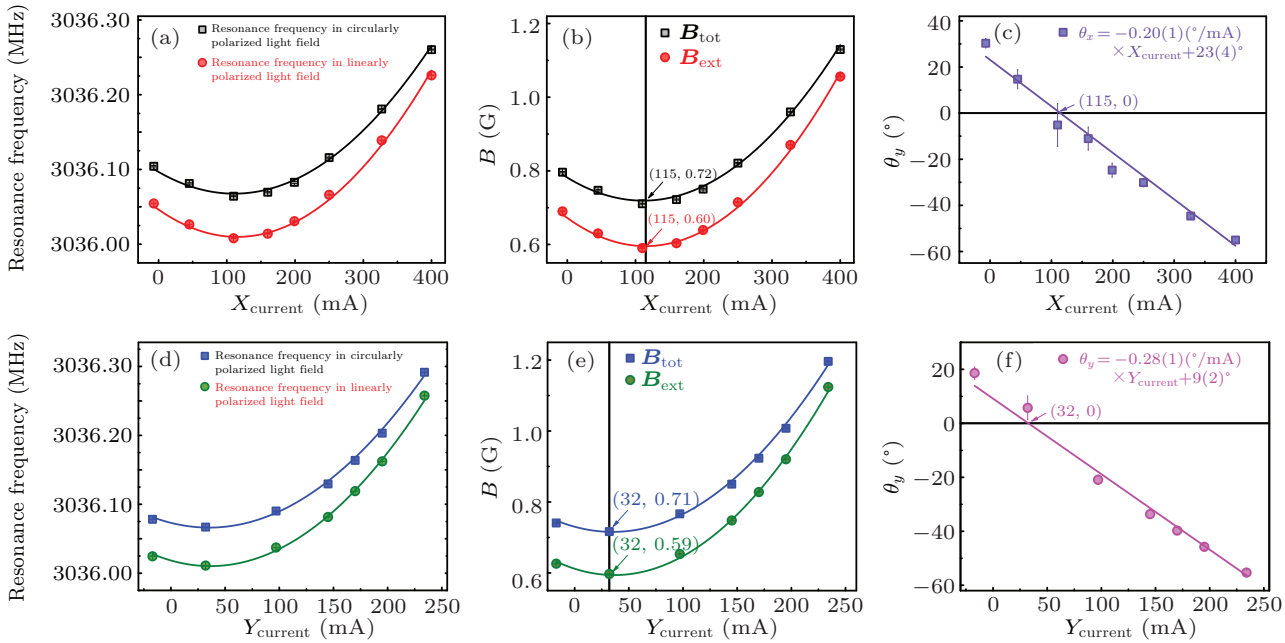


Fig. 2. Dependence of magnetic field and angle on the other two compensating Helmholtz coil currents. (a) The dependence of microwave resonant frequencies in linearly polarized ODTs (red circles) and in fully circularly polarized ODTs (black squares) on $X_{\rm current}$. (b) The dependence of $\boldsymbol{B}_{\rm ext}$ (red circles) in linearly polarized ODTs and the $\boldsymbol{B}_{\rm tot}$ (black squares) in fully circularly polarized ODTs on $X_{\rm current}$. (c) The dependence of θ_x on $X_{\rm current}$. The purple squares are experimental data and the solid line is the fitting curve. (d) The dependence of microwave resonant frequencies in linearly polarized ODTs (green circles) and in fully circularly polarized ODTs (blue squares) on $Y_{\rm current}$. (e) The dependence of $\boldsymbol{B}_{\rm ext}$ (green circles) in linearly polarized ODTs and the $\boldsymbol{B}_{\rm tot}$ (blue squares) in fully circularly polarized ODTs on $Y_{\rm current}$. (f) The dependence of θ_y on $Y_{\rm current}$. The pink circles are experimental data and the solid line is the fitting curve. The data points in these figures are averaged over 50 experimental runs.

(3) **Error introduced by the technical limitations** The currents of the three pairs of Helmholtz coils are actively locked by proportional integral and differential controllers with precise resistors (RS: VPR221T) which serve as feedback sensors. We monitor the current feedback loop that the current drifts by ~ 1‰. The contributions of $\boldsymbol{B}_x$ and $\boldsymbol{B}_y$ to the fluctuation of $\boldsymbol{B}_{\rm ext}$ are $\cos(90° - \theta) \times \Delta \boldsymbol{B}_x$ and $\cos(90° - \theta) \times \Delta \boldsymbol{B}_y$, which are orders of magnitude smaller than the measurement error and nearly negligible. However, the contribution of $\boldsymbol{B}_{\rm bias}$ to the fluctuation of $\boldsymbol{B}_{\rm ext}$ is $\cos(\theta) \times \Delta \boldsymbol{B}_{\rm bias}$, which is not negligible. Thus these parameters introduce the fluctuation of the $\cos(\theta)$ up to 6‰.

(4) **Fitting error of experimental data** The inhomogeneous light shift broadening of the microwave spectrum frequency between states $|0\rangle$ and $|5s_{1/2}, F = 3, m_F = 1\rangle$ is 1‰, which is linear with Zeeman shift $g_{\rm F}\mu_{\rm B} m_F \boldsymbol{B}$. Thus the fitting errors of the $\boldsymbol{B}_{\rm ext}$ and $\boldsymbol{B}_{\rm tot}$ are 1‰ and the fluctuation of $\cos(\theta)$ is 6‰. All sources of errors combine to give a $\sim 4\%$ fluctuation of the compensated value of θ_x (θ_y), consistent with the measurement result.

To further verify the differences between the calibrated and uncalibrated angles and the calibration accuracy of the compensating technique, we observe the Rabi oscillations between $|0\rangle$ and $|5s_{1/2}, F = 3, m_F = 0\rangle$ states of ^{85}Rb qubits in both the linearly and circularly polarized ODTs. Rabi oscillations on Zeeman-insensitive transition are recorded at a trap depth of $h \times (-10.0\,\text{MHz})$. The $\boldsymbol{B}_{\rm fict} = -0.10(1)\,(\text{G/MHz}) \times U_{\rm a}$ is about 1.00 G, which is the same order of magnitude as the $\boldsymbol{B}_{\rm ext}$. We fit the experimental data in Fig. 3(a) with $P(t) = C[1 - \cos(\Omega_{\rm R} t)]/2$, which yields Rabi frequencies of $\Omega_{\rm R}/(2\pi) = 7.2(1)$ kHz in a linearly polarized ODT and $\Omega_{\rm R}/(2\pi) = 15.9(1)$ kHz in a circularly polarized ODT before implementing the compensating magnetic fields. Owing to the $\boldsymbol{B}_{\rm fict}$ induced by the circularly polarized trapping laser, the direction of the quantization axis is different from that in the linearly polarized ODT. Consequently, the projection value of the microwave antenna on the quantization axis varies in ODTs with different polarizations, which leads to inconsistent Rabi frequencies. In addition, the dephasing of Rabi oscillation in circularly polarized ODTs is due to the impurity of the degree of trapping laser polarization, which is caused by the original angle between the $\boldsymbol{B}_{\rm bias}$ and the propagating direction of the light field for trapping neutral atoms. After applying the compensating magnetic fields of the X- and Y-axis with $X_{\rm current} = 115$ mA and $Y_{\rm current} = 32$ mA, the Rabi frequency of the Zeeman-insensitive transition in circularly polarized ODTs is almost the same as that in linearly polarized ODTs, as verified by the experimental data in Fig. 3(b); the Rabi frequencies are 5.4(2) kHz and 5.7(1) kHz, respectively. The maximum population detected in state $|0\rangle$ is 90(5)% in Fig. 3. This evident decrement, as observed from 100%, is caused by two reasons. One is that some atoms are lost before the state-selective

detection due to atoms heating in the ODTs. The other reason is the imperfect optical pumping process.

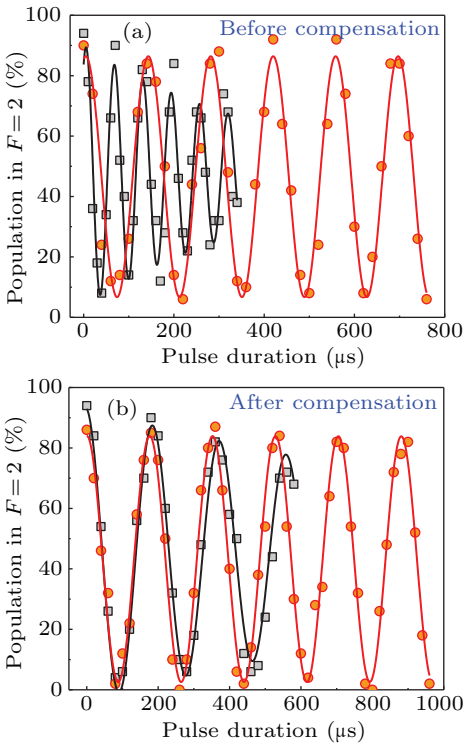


Fig. 3. Rabi oscillations in linearly polarized ODTs (red dots) and circularly polarized ODTs (black squares) before and after implementing the compensating magnetic fields in the other two directions orthogonal to $\boldsymbol{B}_{\rm bias}$ direction. (a) Before applying the compensating magnetic fields, the relative difference of Rabi frequencies in linearly and circularly polarized ODTs is 0.377(7) with $\theta_x = 23(4)^\circ$ and $\theta_y = 9(2)^\circ$. In addition, the lifetime of the Rabi oscillation in linearly polarized ODTs is about 433 μs. (b) After the compensation, the relative difference has been reduced to almost zero with $\theta_x = 0(4)^\circ$ and $\theta_y = 0(4)^\circ$, which also substantially enhances the lifetime of the Rabi oscillation in linearly polarized ODT to 1464 μs. The data points in this figure are averaged over 50 experimental runs.

5. Conclusion

In conclusion, we have presented a novel *in situ* method to calibrate the angle between the quantization axis and the propagating direction of a tightly-focused trapping laser. With this method, the projected value of the angle on either of the compensating planes is reduced to $0(4)^\circ$, which is very important for the accurate measurement of hyperpolarizability in magic-intensity ODTs. Moreover, when the original angle is reduced to nearly zero, the projected value of the microwave power on the quantization axis is a constant, which is beneficial to the coherent manipulation of single qubits in magic-intensity ODT arrays. Our method can be straightforwardly extended to other similar precision measurements with trapped neutral atoms, e.g., cancellation of the angle between circularly polarized Rydberg excitation lasers and the quantization axis.[38]

Acknowledgements

Project supported by the National Natural Science Foundation of China (Grant Nos. 12104414, 12122412, 12104464, and 12104413) and the China Postdoctoral Science Foundation (Grant No. 2021M702955).

References

[1] Bloch I, Dalibard J and Nascimbène S 2012 *Nat. Phys.* **8** 267
[2] Georgescu I M, Ashhab S and Nori F 2014 *Rev. Mod. Phys.* **86** 153
[3] Saffman M, Walker T G and Mölmer K 2010 *Rev. Mod. Phys.* **82** 2313
[4] Negretti A, Treutlein P and Calarco T 2011 *Quantum Inf. Process.* **10** 721
[5] Saffman M 2016 *J. Phys. B: At. Mol. Opt. Phys.* **49** 202001
[6] Weiss D S and Saffman M 2017 *Phys. Today* **70** 44
[7] Derevianko A and Katori H 2011 *Rev. Mod. Phys.* **83** 331
[8] Escher B M, de Matos Filho R L and Davidovich L 2011 *Nat. Phys.* **7** 406
[9] Giovannetti V, Lloyd S and Maccone L 2011 *Nat. Photon.* **5** 222
[10] Romalis M V and Fortson E N 1999 *Phys. Rev. A* **59** 4547
[11] Kuhr S, Alt W, Schrader D, Dotsenko I, Miroshnychenko Y, Rosenfeld W, Khudaverdyan M, Gomer V, Rauschenbeutel A and Meschede D 2003 *Phys. Rev. Lett.* **91** 213002
[12] Kuhr S, Alt W, Schrader D, Dotsenko I, Miroshnychenko Y, Rauschenbeutel A and Meschede D 2005 *Phys. Rev. A* **72** 023406
[13] Yu S, Xu P, He X D, Liu M, Wang J and Zhan M S 2013 *Opt. Express* **21** 32130
[14] Carr A W and Saffman M 2016 *Phys. Rev. Lett.* **117** 150801
[15] Yang J H, He X D, Guo R J, Xu P, Wang K P, Sheng C, Liu M, Wang J, Derevianko A and Zhan M S 2016 *Phys. Rev. Lett.* **117** 123201
[16] Sheng C, He X D, Xu P, Guo R J, Wang K P, Xiong Z Y, Liu M, Wang J and Zhan M S 2018 *Phys. Rev. Lett.* **121** 240501
[17] Xin M J, Leong W S, Chen Z L and Lan S Y 2019 *Phys. Rev. Lett.* **122** 163901
[18] Guo R J, He X D, Sheng C, Yang J H, Xu P, Wang K P, Zhong J Q, Liu M, Wang J and Zhan M S 2020 *Phys. Rev. Lett.* **124** 153201
[19] Cohen-Tannoudji C and Dupont-Roc J 1972 *Phys. Rev. A* **5** 968
[20] Rosatzin M, Suter D and Mlynek J 1990 *Phys. Rev. A* **42** 1839
[21] Zielonkowski M, Steiger J, Schünemann U, DeKieviet M and Grimm R 1998 *Phys. Rev. A* **58** 3993
[22] Park C Y, Kim J Y, Song J M and Cho D 2002 *Phys. Rev. A* **65** 033410
[23] Yang G Q, Yan H, Shi T, Wang J and Zhan M S 2008 *Phys. Rev. A* **78** 033415
[24] Zhu K, Solmeyer N, Tang C and Weiss D S 2013 *Phys. Rev. Lett.* **111** 243006
[25] Le Kien F, Schneeweiss P and Rauschenbeutel A 2013 *Eur. Phys. J. D* **67** 92
[26] Schneeweiss P, Le Kien F and Rauschenbeutel A 2014 *New J. Phys.* **16** 013014
[27] Albrecht B, Meng Y, Clausen C, Dareau A, Schneeweiss P and Rauschenbeutel A 2016 *Phys. Rev. A* **94** 061401
[28] Dareau A, Meng Y, Schneeweiss P and Rauschenbeutel A 2018 *Phys. Rev. Lett.* **121** 253603
[29] Leszczyński A, Mazelanik M, Lipka M, Parniak M, Dabrowski M and Wasilewski W 2018 *Opt. Lett.* **43** 1147
[30] Wang K P, Zhuang J, He X D, Guo R J, Sheng C, Xu P, Liu M, Wang J and Zhan M S 2020 *Chin. Phys. Lett.* **37** 044209
[31] Martínez-Dorantes M, Alt W, Gallego J, Ghosh S, Ratschbacher L, Völzke Y and Meschede D 2017 *Phys. Rev. Lett.* **119** 180503
[32] Kwon M, Ebert M F, Walker T G and Saffman M 2017 *Phys. Rev. Lett.* **119** 180504
[33] Martínez-Dorantes M 2016 *Fast Non-destructive Internal State Detection of Neutral Atoms in Optical Potentials* (Ph.D. Dissertation) (Bonn: Rheinischen Friedrich-Wilhelms-Universität Bonn)
[34] Schlosser N, Reymond G, Protsenko I and Grangier P 2001 *Nature* **411** 1024
[35] Schlosser N, Reymond G and Grangier P 2002 *Phys. Rev. Lett.* **89** 023005
[36] Breit G and Rabi I I 1931 *Phys. Rev.* **38** 2082
[37] Moskovkin D L and Shabaev V M 2006 *Phys. Rev. A* **73** 052506
[38] Zeng Y, Xu P, He X D, Liu Y Y, Liu M, Wang J, Papoular D J, Shlyapnikov G V and Zhan M S 2017 *Phys. Rev. Lett.* **119** 160502